

NLO corrections to Vector Dark Matter Direct Detection - An update

Seraina Glaus

Institute for Theoretical Physics, Karlsruhe Institute of Technology, 76128 Karlsruhe, Germany

Institute for Nuclear Physics, Karlsruhe Institute of Technology, 76344 Karlsruhe, Germany

E-mail: seraina.glaus@kit.edu

Margarete Mühlleitner

Institute for Theoretical Physics, Karlsruhe Institute of Technology, 76128 Karlsruhe, Germany

E-mail: milada.muehlleitner@kit.edu

Jonas Müller

Institute for Theoretical Physics, Karlsruhe Institute of Technology, 76128 Karlsruhe, Germany

E-mail: jonas.mueller@kit.edu

Shruti Patel

Institute for Theoretical Physics, Karlsruhe Institute of Technology, 76128 Karlsruhe, Germany

Institute for Nuclear Physics, Karlsruhe Institute of Technology, 76344 Karlsruhe, Germany

E-mail: shruti.patel@kit.edu

Rui Santos^{*†}

Centro de Física Teórica e Computacional, Faculdade de Ciências,

Universidade de Lisboa, Campo Grande, Edifício C8 1749-016 Lisboa, Portugal, and

ISEL - Instituto Superior de Engenharia de Lisboa,

Instituto Politécnico de Lisboa 1959-007 Lisboa, Portugal.

E-mail: rasantos@fc.ul.pt

In this work we present an update to a previous calculation of the Next-to-Leading Order (NLO) corrections to the Vector Dark Matter (VDM) direct detection cross section. The model under investigation is a minimal extension of the Standard Model (SM) with one extra vector boson and one extra complex scalar field, where the vector is the DM candidate. We have computed the spin-independent cross section for the scattering of the VDM particle with a nucleon. We now provide an update to the NLO cross section for the direct detection of the DM particle. We further discuss the phenomenological implications of the NLO corrections for the sensitivity of the direct detection DM experiments.

Corfu Summer Institute 2019 "School and Workshops on Elementary Particle Physics and Gravity" (CORFU2019)

31 August - 25 September 2019

Corfú, Greece

^{*}Speaker.

[†]I would like to thank the organisers for their partial support.

1. Introduction

The experimental evidence for the existence of Dark Matter (DM) can be traced back to the work of Zwicky [1], "The redshift of extragalactic nebulae". Many experimental results from different sources and origins have been accumulated over the years leading to the conclusion that 27% of the energy density of the Universe is unaccounted for in the Standard Model (SM) of particle physics, and this missing dark matter is most likely a particle. These results are all gravitational in origin which means that the properties of dark matter are dictated by Astronomy and Cosmology. If DM is indeed a particle it could be produced at colliders, but signatures of missing energy alone cannot be a proof of the existence of DM. Indirect searches for DM annihilation can also hint at the existence of DM and in the worst case scenario they can at least be used to exclude specific models or regions of their parameter space. Direct DM detection is our best hope to unambiguously find a dark matter candidate and it is therefore the place where precision matters the most. When searching for DM in direct detection, all available experimental data combined favours a weakly interacting massive particle (WIMP) with a velocity of the order of 200 km/s. In this work we discuss a minimal model which is an extension of the SM by the addition of a dark vector χ_μ with a gauged $U(1)_\chi$ symmetry and a complex SM-gauge singlet S . We will call this model Vector Dark Matter (VDM) in the following.

As shown in [2], DM particles that undergo coherent scattering with nuclei are the easiest to detect due the larger scattering rates. There are many uncertainties from cosmological and astronomical origins but particle physicists have tried to increase precision from their side by calculating higher-order corrections to the scattering cross sections, both strong and electroweak [3–13]. The electroweak corrections to the coherent scattering of the DM candidate χ_μ require the renormalisation of the VDM model. After renormalisation, the coefficients from each term in the spin-independent amplitude, with renormalised loop corrections included, are matched to the effective couplings of the Lagrangian, \mathcal{L}_{eff} , which describes the coupling of two DM particles with two quarks. These will be the corrected coefficients to the corresponding tree-level effective couplings from \mathcal{L}_{eff} .

Most of the work presented here was published in Ref. [13]. We have extended the work by calculating one-loop corrections to the $\bar{q}qh$ vertex. This will be discussed in detail in Sec. 4.5. The main conclusions are the same as in our previous work [13], except for a slight reduction in the overall NLO corrections relative to the LO result.

2. The Vector Dark Matter Model

In this section we briefly review our VDM model and refer the reader to Refs. [13–21] for details. The model has two new fields relative to the SM: one vector boson and one complex scalar singlet. Besides the SM symmetries there is now a new $U(1)_\chi$ gauge symmetry under which all SM fields are neutral. The new singlet is a scalar under the SM gauge group but has unit charge under $U(1)_\chi$. The appearance of the new dark gauge boson, named χ_μ , is a consequence of the gauged $U(1)_\chi$ symmetry. In order to have a stable VDM candidate we further force the model to be invariant under the \mathbb{Z}_2 symmetry,

$$X_\mu \rightarrow -X_\mu, \quad S \rightarrow S^* \tag{2.1}$$

for the dark gauge boson χ_μ and for the singlet field \mathbb{S} . The SM particles are all even under \mathbb{Z}_2 , and therefore there is no kinetic mixing between the gauge bosons from $U(1)_\chi$ and from the SM $U(1)_Y$. The complete Lagrangian of the theory is

$$\mathcal{L} = \mathcal{L}_{SM} - \frac{1}{4} X_{\mu\nu} X^{\mu\nu} + (D_\mu \mathbb{S})^\dagger (D^\mu \mathbb{S}) + \mu_S^2 |\mathbb{S}|^2 - \lambda_S |\mathbb{S}|^4 - \kappa |\mathbb{S}|^2 H^\dagger H, \quad (2.2)$$

where $X^{\mu\nu}$ is the $U(1)_\chi$ field-strength tensor and the covariant derivative

$$D_\mu \mathbb{S} = (\partial_\mu + ig_\chi \chi_\mu) \mathbb{S}, \quad (2.3)$$

with g_χ being the gauge coupling of the dark gauge boson χ_μ . The mass and coupling parameters μ_S^2 , λ_S and κ are all real. The SM potential has the form $V_{SM} = -\mu_H^2 |H|^2 + \lambda_H |H|^4$. Both the neutral component of the doublet H and the real part of the singlet field \mathbb{S} acquire vacuum expectation values (VEV) v and v_S , respectively. They are expanded around their VEVs as

$$H = \begin{pmatrix} G^+ \\ \frac{1}{\sqrt{2}} (v + \Phi_H + i\sigma_H) \end{pmatrix} \quad \text{and} \quad \mathbb{S} = \frac{1}{\sqrt{2}} (v_S + \Phi_S + i\sigma_S), \quad (2.4)$$

where Φ_H and Φ_S denote the CP-even field components of H and \mathbb{S} , respectively.

The imaginary components of the doublet, σ_H , and of the singlet, σ_S , are the neutral SM-like Goldstone boson G^0 and the Goldstone boson G^χ for the gauge boson χ_μ , respectively. The charged Goldstone boson, partner of the W^\pm boson, is G^\pm . We write the minimum conditions as

$$\left\langle \frac{\partial V}{\partial \Phi_H} \right\rangle \equiv \frac{T_{\Phi_H}}{v} = \left(\frac{\kappa v_S^2}{2} + \lambda_H v^2 - \mu_H^2 \right), \quad (2.5)$$

$$\left\langle \frac{\partial V}{\partial \Phi_S} \right\rangle \equiv \frac{T_{\Phi_S}}{v_S} = \left(\frac{\kappa v^2}{2} + \lambda_S v_S^2 - \mu_S^2 \right), \quad (2.6)$$

which in turn allows us to express the mass matrix of the scalar particles as

$$\mathcal{M}_{\Phi_h \Phi_S} = \begin{pmatrix} 2\lambda_H v^2 & \kappa v v_S \\ \kappa v v_S & 2\lambda_S v_S^2 \end{pmatrix} + \begin{pmatrix} \frac{T_{\Phi_H}}{v} & 0 \\ 0 & \frac{T_{\Phi_S}}{v_S} \end{pmatrix}. \quad (2.7)$$

The CP-even mass eigenstates h_1 and h_2 are then obtained via the rotation matrix R_α as

$$\begin{pmatrix} h_1 \\ h_2 \end{pmatrix} = R_\alpha \begin{pmatrix} \Phi_H \\ \Phi_S \end{pmatrix} \equiv \begin{pmatrix} \cos \alpha & \sin \alpha \\ -\sin \alpha & \cos \alpha \end{pmatrix} \begin{pmatrix} \Phi_H \\ \Phi_S \end{pmatrix}. \quad (2.8)$$

The physical scalar states are h_1 and h_2 with masses m_{h_1} and m_{h_2} . Denoting the mass of the VDM particle by m_χ we choose the following set of independent parameters

$$m_{h_1}, m_{h_2}, m_\chi, \alpha, v, g_\chi, T_{\Phi_H}, T_{\Phi_S}. \quad (2.9)$$

The remaining parameters can be written as a function of this set as

$$\lambda_H = \frac{m_{h_1}^2 \cos^2 \alpha + m_{h_2}^2 \sin^2 \alpha}{2v^2}, \quad (2.10)$$

$$\kappa = \frac{(m_{h_1}^2 - m_{h_2}^2) \cos \alpha \sin \alpha}{v v_S}, \quad (2.11)$$

$$\lambda_S = \frac{m_{h_1}^2 \sin^2 \alpha + m_{h_2}^2 \cos^2 \alpha}{2v_S}, \quad (2.12)$$

$$v_S = \frac{m_\chi}{g_\chi}. \quad (2.13)$$

The SM VEV $v \approx 246$ GeV is fixed by the W boson mass and the mixing angle α is varied in the interval $-\frac{\pi}{2} \leq \alpha < \frac{\pi}{2}$. We require the potential to be in a global minimum, that perturbative unitarity holds and enforce the potential to be bounded from below implying the conditions,

$$\lambda_H > 0, \quad \lambda_S > 0, \quad \kappa > -2\sqrt{\lambda_H \lambda_S}. \quad (2.14)$$

2.1 Renormalisation of the VDM Model

In this section we briefly highlight the renormalisation procedure and direct the reader to Ref. [13] for details. There are four new parameters relative to the SM that need to be renormalised: the non-SM-like scalar mass, m_{h_2} , the rotation angle α , the coupling g_χ and the DM mass m_χ .¹ Our renormalisation procedure is the following. Once the free parameters are chosen we replace the bare parameters p_0 with the renormalised ones p according to

$$p_0 = p + \delta p, \quad (2.15)$$

where δp is the counterterm for the parameter p . The fields Ψ are renormalised multiplicatively,

$$\Psi_0 = \sqrt{Z_\Psi} \Psi, \quad (2.16)$$

where Z_Ψ is the field renormalisation constant and Ψ_0 stands for the bare field and Ψ for the renormalised field. When there is mixing like is the case for our scalar sector, $\sqrt{Z_\Psi}$ is a matrix.

The renormalisation of the SM is by now a textbook subject. Therefore we will discuss only the renormalisation of the extra parameters of the model. In the gauge sector there is just one extra field, that is, one extra mass renormalisation constant and one field renormalisation constant. Furthermore, the \mathbb{Z}_2 symmetry under which only the dark gauge boson χ_μ is odd, precludes kinetic mixing between the gauge bosons of the $U(1)_\chi$ and that of the $U(1)_Y$. Since the symmetry is broken only spontaneously this is true to all orders in perturbation theory. We define $m_\chi^2 \rightarrow m_\chi^2 + \delta m_\chi^2$ and $\chi \rightarrow (1 + \frac{1}{2} \delta Z_{\chi\chi}) \chi$ and the on-shell (OS) conditions yield the following expressions for the counterterms

$$\delta Z_{\chi\chi} = -\text{Re} \left. \frac{\partial \Sigma_{\chi\chi}^T(p^2)}{\partial p^2} \right|_{p^2=m_\chi^2}, \quad \text{and} \quad \delta m_\chi^2 = \text{Re} \Sigma_{\chi\chi}^T(m_\chi^2), \quad (2.17)$$

where the subscript T identifies the transverse part of the self-energies

The dark gauge coupling g_χ cannot be measured directly in a physical process and we have therefore decided to renormalise it using the $\overline{\text{MS}}$ scheme. We choose the triple vertex $h_1 h_1 h_1$ to determine g_χ (the UV divergence is universal). Defining

$$\mathcal{A}_{h_1 h_1 h_1}^{\text{NLO}} = \mathcal{A}_{h_1 h_1 h_1}^{\text{LO}} + \mathcal{A}_{h_1 h_1 h_1}^{\text{VC}} + \mathcal{A}_{h_1 h_1 h_1}^{\text{CT}}, \quad (2.18)$$

¹Note that in our notation h_1 corresponds to the SM-like Higgs boson, while we attribute h_2 to the non-SM-like scalar.

where \mathcal{A}^{VC} and \mathcal{A}^{CT} are the amplitude for the virtual corrections and vertex counterterms, respectively. Dropping the index $h_1 h_1 h_1$, the counterterm amplitude can be written as

$$\mathcal{A}^{\text{CT}} = \delta^{\text{mix}} + \delta g^{\text{CT}} \quad (2.19)$$

with

$$\delta^{\text{mix}} = \frac{3}{2} g_{h_1 h_1 h_1} \delta Z_{h_1 h_1} + \frac{3}{2} g_{h_1 h_1 h_2} \delta Z_{h_2 h_1} \quad (2.20)$$

The trilinear Higgs self-coupling reads

$$g_{h_1 h_1 h_1} = -\frac{3gm_{h_1}^2}{2m_W} \cos^3 \alpha - \frac{3g_\chi m_{h_1}^2}{m_\chi} \sin^3 \alpha. \quad (2.21)$$

and the corresponding CTs are

$$\delta g^{\text{CT}} = \sum_p \frac{\partial g_{h_1 h_1 h_1}}{\partial p} \delta p, \quad p = m_{h_1}^2, m_\chi^2, m_W^2, g, \alpha, g_\chi. \quad (2.22)$$

The divergent part of δg_χ is then given by

$$\delta g_\chi \Big|_{\text{div}} = \left(\frac{m_\chi}{3m_{h_1}^2 \sin^3 \alpha} \right) \left(\mathcal{A}^{\text{VC}} + \mathcal{A}^{\text{CT}} \Big|_{\delta g_\chi=0} \right) \Big|_{\text{div}}, \quad (2.23)$$

where $(\dots)_{\text{div}}$ indicates the UV pole.

The one-loop diagrams were generated with `FeynArts` [22] for which the model file was obtained with `SARAH` [23–26] and the program packages `FeynCalc` [27,28] and `FormCalc` [29] were used to reduce the amplitudes to Passarino-Veltmann integrals [30]. The numerical evaluation of the integrals was done by `Collier` [31–34]. The counterterm g_χ in the $\overline{\text{MS}}$ scheme is then obtained as

$$\delta g_\chi \Big|_\varepsilon = \frac{g_\chi^3}{96\pi^2} \Delta_\varepsilon, \quad (2.24)$$

with

$$\Delta_\varepsilon = \frac{1}{\varepsilon} - \gamma_E + \ln 4\pi, \quad (2.25)$$

where γ_E denotes the Euler-Mascheroni constant.

We end this section with the renormalisation of the scalar sector. Relative to the SM we have a new field, the real component Φ_S of the singlet, which mixes with the real neutral Φ_H of the Higgs doublet. These two fields mix giving rise to two mass eigenstates h_1 and h_2 and a mixing angle α . Hence, the field renormalisation constants are now written as

$$\begin{pmatrix} h_1 \\ h_2 \end{pmatrix} \rightarrow \begin{pmatrix} 1 + \frac{1}{2} \delta Z_{h_1 h_1} & \frac{1}{2} \delta Z_{h_1 h_2} \\ \frac{1}{2} \delta Z_{h_2 h_1} & 1 + \frac{1}{2} \delta Z_{h_2 h_2} \end{pmatrix} \begin{pmatrix} h_1 \\ h_2 \end{pmatrix}. \quad (2.26)$$

In the mass eigenbasis, the mass matrix in Eq. (2.7) yields

$$\mathcal{M}_{h_1 h_2} = \underbrace{\begin{pmatrix} m_{h_1}^2 & 0 \\ 0 & m_{h_2}^2 \end{pmatrix}}_{\equiv \mathcal{M}^2} + R_\alpha \underbrace{\begin{pmatrix} T_{\Phi_H}/v & 0 \\ 0 & T_{\Phi_S}/v_S \end{pmatrix}}_{\equiv \delta T} R_\alpha^T. \quad (2.27)$$

The tadpole terms in the tree-level mass matrix are *bare parameters*. Therefore we first have to renormalise the tadpoles in such a way that the theory has a minimum at next-to-leading order (NLO). The tadpole renormalisation condition counterterms is defined as

$$\hat{T}_i = T_i - \delta T_i \stackrel{!}{=} 0, \quad i = \Phi_H, \Phi_S, \quad (2.28)$$

where \hat{T}_i is the one-loop renormalised tadpole. In the mass basis the tadpole counterterms are written as

$$\begin{pmatrix} T_{h_1} \\ T_{h_2} \end{pmatrix} = R_\alpha \cdot \begin{pmatrix} T_{\Phi_H} \\ T_{\Phi_S} \end{pmatrix}. \quad (2.29)$$

which in turn implies

$$\delta \mathcal{M}_{h_1 h_2} = \begin{pmatrix} \delta m_{h_1}^2 & 0 \\ 0 & \delta m_{h_2}^2 \end{pmatrix} + R_\alpha \begin{pmatrix} \frac{\delta T_{\Phi_H}}{v} & 0 \\ 0 & \frac{\delta T_{\Phi_S}}{v_S} \end{pmatrix} R_\alpha^T \equiv \begin{pmatrix} \delta m_{h_1}^2 & 0 \\ 0 & \delta m_{h_2}^2 \end{pmatrix} + \begin{pmatrix} \delta T_{h_1 h_1} & \delta T_{h_1 h_2} \\ \delta T_{h_2 h_1} & \delta T_{h_2 h_2} \end{pmatrix}, \quad (2.30)$$

In Eq. (2.30) we neglect all terms of order $\mathcal{O}(\delta\alpha\delta T_i)$ since they are formally of two-loop order. Using OS conditions and Eq. (2.30) finally yields the following relations for the counterterms ($i = 1, 2$)

$$\delta m_{h_i}^2 = \text{Re}[\Sigma_{h_i h_i}(m_{h_i}^2) - \delta T_{h_i h_i}], \quad (2.31)$$

$$\delta Z_{h_i h_i} = -\text{Re} \left[\frac{\partial \Sigma_{h_i h_i}(p^2)}{\partial p^2} \right]_{p^2=m_{h_i}^2}, \quad (2.32)$$

$$\delta Z_{h_i h_j} = \frac{2}{m_{h_i}^2 - m_{h_j}^2} \text{Re}[\Sigma_{h_i h_j}(m_{h_j}^2) - \delta T_{h_i h_j}], \quad i \neq j. \quad (2.33)$$

We now move to the final parameter that needs to be renormalised, the mixing angle α . There are processes that depend on the mixing angle and so one option is to use one such process. This leads, however, to unphysically large counterterms [35]. The renormalisation of the mixing angles in SM extensions was thoroughly discussed in [35–46]. In this work we will use the scheme proposed in [47, 48], which connects the derivation of the angle counterterm with the usual OS conditions of the scalar field to the relations between the gauge basis and the mass basis. The bare parameter expressed through the renormalised one and the counterterm reads

$$\alpha_0 = \alpha + \delta\alpha. \quad (2.34)$$

Considering the field strength renormalisation before the rotation,

$$\begin{pmatrix} h_1 \\ h_2 \end{pmatrix} = R(\alpha + \delta\alpha) \sqrt{Z_\Phi} \begin{pmatrix} \Phi_H \\ \Phi_S \end{pmatrix}, \quad (2.35)$$

and expanding it to strict one-loop order,

$$R(\alpha + \delta\alpha) \sqrt{Z_\Phi} \begin{pmatrix} \Phi_H \\ \Phi_S \end{pmatrix} = \underbrace{R(\delta\alpha)R(\alpha)\sqrt{Z_\Phi}R(\alpha)^T R(\alpha)}_{\stackrel{!}{=} \sqrt{Z_H}} \begin{pmatrix} \Phi_H \\ \Phi_S \end{pmatrix} + \mathcal{O}(\delta\alpha^2) = \sqrt{Z_H} \begin{pmatrix} h_1 \\ h_2 \end{pmatrix}, \quad (2.36)$$

yields the field strength renormalisation matrix $\sqrt{Z_H}$ connecting the bare and renormalised fields in the mass basis. This finally leads to the condition [35]

$$\delta\alpha = \frac{1}{4}(\delta Z_{h_1 h_2} - \delta Z_{h_2 h_1}) \quad (2.37)$$

$$= \frac{1}{2(m_{h_1}^2 - m_{h_2}^2)} \text{Re}(\Sigma_{h_1 h_2}(m_{h_1}^2) + \Sigma_{h_1 h_2}(m_{h_2}^2) - 2\delta T_{h_1 h_2}) . \quad (2.38)$$

In the numerical analysis presented in our work [13] we have used two further renormalisation schemes for $\delta\alpha$: the $\overline{\text{MS}}$ scheme and a process-dependent scheme. The results presented here use, however, only the scheme previously described.

3. Dark Matter Direct Detection at Tree Level

The spin-independent (SI) cross section of DM-nucleon scattering can be described with an effective Lagrangian. The largest contributions to the cross section are due to light quarks $q = u, d, s$ and gluons. In the VDM model the SI cross section is well described by an effective operator Lagrangian [49]

$$\mathcal{L}^{\text{eff}} = \sum_{q=u,d,s} \mathcal{L}_q^{\text{eff}} + \mathcal{L}_G^{\text{eff}} , \quad (3.1)$$

with

$$\mathcal{L}_q^{\text{eff}} = f_q \chi_\mu \chi^\mu m_q \bar{q} q + \frac{g_q}{m_\chi^2} \chi^\rho i \partial^\mu i \partial^\nu \chi_\rho \mathcal{O}_{\mu\nu}^q , \quad (3.2a)$$

$$\mathcal{L}_G^{\text{eff}} = f_G \chi_\rho \chi^\rho G_{\mu\nu}^a G^{a\mu\nu} , \quad (3.2b)$$

where $G_{\mu\nu}^a$ ($a = 1, \dots, 8$) is the gluon field strength tensor and $\mathcal{O}_{\mu\nu}^q$ is the quark twist-2 operator corresponding to the traceless part of the energy-momentum tensor of the nucleon [50, 51],

$$\mathcal{O}_{\mu\nu}^q = \frac{1}{2} \bar{q} i \left(\partial_\mu \gamma_\nu + \partial_\nu \gamma_\mu - \frac{1}{2} \not{\partial} \right) q . \quad (3.3)$$

In our calculation we will neglect operators suppressed by the DM velocities and also the gluon twist-2 operator $\mathcal{O}_{\mu\nu}^g$, because they are one order higher in the strong coupling constant α_s [49].

Taking the nucleon states to be on-shell and considering vanishing momentum transfer, the nucleon matrix elements are given by

$$\langle N | m_q \bar{q} q | N \rangle = m_N f_{T_q}^N \quad (3.4a)$$

$$-\frac{9\alpha_s}{8\pi} \langle N | G_{\mu\nu}^a G^{a,\mu\nu} | N \rangle = \left(1 - \sum_{q=u,d,s} f_{T_q}^N \right) m_N = m_N f_{T_G}^N \quad (3.4b)$$

$$\langle N(p) | \mathcal{O}_{\mu\nu}^q | N(p) \rangle = \frac{1}{m_N} \left(p_\mu p_\nu - \frac{1}{4} m_N^2 g_{\mu\nu} \right) (q^N(2) + \bar{q}^N(2)) , \quad (3.4c)$$

where N stands for a nucleon, $N = p, n$, and m_N is the nucleon mass and p is the four-momentum of the nucleon. The fraction of momentum carried by the quarks is determined by the second moments, $q^N(2)$ and $\bar{q}^N(2)$, of the parton distribution functions of the quark $q(x)$ and the antiquark

$\bar{q}(x)$, respectively. $f_{T_q}^N, f_{T_G}^N$ denote the fraction of the nucleon mass that is due to light quarks q or to the gluon, respectively. These are obtained from lattice calculations and are given in App. A.

The SI scattering DM-nucleon cross section can now be written as

$$\sigma_N = \frac{1}{\pi} \left(\frac{m_N}{m_\chi + m_N} \right)^2 |f_N|^2, \quad (3.5)$$

where the nucleon is either a proton or a neutron ($N = p, n$) and

$$f_N/m_N = \sum_{q=u,d,s} f_q f_{T_q}^N + \sum_{q=u,d,s,c,b} \frac{3}{4} (q^N(2) + \bar{q}^N(2)) g_q - \frac{8\pi}{9\alpha_S} f_{T_G}^N f_G. \quad (3.6)$$

In the contribution from the quark twist-2 operator all quarks below the energy scale ~ 1 GeV have to be included, *i.e.* all quarks but the top quark. The sum in the first term of Eq. (3.6) is only

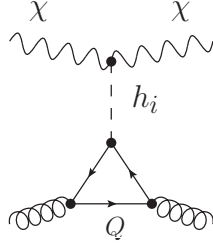


Figure 1: Higgs bosons h_i mediating the coupling of two gluons to two VDM particles through a heavy quark loop.

over the light quarks. There is, however, a leading-order gluon interaction through a heavy quark triangle diagram, *cf.* Fig. 1, with a charm, bottom or top quark in the loop. Since their mass is above the energy scale relevant for DM direct detection, they should be integrated out for the description of the interaction at the level of the nucleon. This is done by calculating the heavy quark triangle diagrams and then integrating out the heavy quarks. The procedure is equivalent to calculating the amplitude in Fig. 2 with heavy quarks $Q = c, b, t$, and replacing the resulting tensor structure $m_Q \bar{Q}Q$ with the effective gluon operator [11, 12, 52]

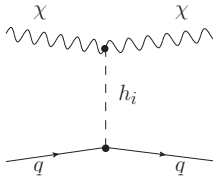


Figure 2: Generic tree-level diagram contribution to the SI cross section. The mediator h_i corresponds to the two Higgs bosons h_1 and h_2 . The quark line q corresponds to all quarks $q = u, d, s, c, b, t$.

$$m_Q \bar{Q}Q \rightarrow -\frac{\alpha_S}{12\pi} G_{\mu\nu}^a G^{a\mu\nu}, \quad (3.7)$$

corresponding to the effective leading-order VDM-gluon interaction in Eq. (3.2).

The tree-level diagrams contributing to the SI cross section are shown in Fig. 2 and are calculated for vanishing momentum transfer. The Wilson coefficient for each effective operator in

Eq. (3.1) is extracted by projecting onto the corresponding tensor structure, $m_q q \bar{q}$, leading to

$$f_q = \frac{1}{2} \frac{g g_\chi}{m_W} \frac{\sin(2\alpha)}{2} \frac{m_{h_1}^2 - m_{h_2}^2}{m_{h_1}^2 m_{h_2}^2} m_\chi, \quad q = u, d, s, c, b, t. \quad (3.8)$$

As previously discussed, the heavy quarks $Q = b, c, t$ contribute to the effective gluon interaction and using Eq. (3.7), the Wilson coefficient for the gluon interaction, f_G , can be written in terms of f_q for $q = c, b, t$,

$$f_G = \sum_{q=c,b,t} -\frac{\alpha_S}{12\pi} f_q, \quad (3.9)$$

resulting in the SI LO cross section

$$\sigma^{\text{LO}} = \frac{\sin^2 2\alpha}{4\pi} \left(\frac{m_\chi m_N}{m_\chi + m_N} \right)^2 \frac{(m_{h_1}^2 - m_{h_2}^2)^2}{m_{h_1}^4 m_{h_2}^4} \frac{m_\chi^2 m_N^2}{v^2 v_S^2} \left| \sum_{q=u,d,s} f_{T_q}^N + 3 \cdot \frac{2}{27} f_{T_G}^N \right|^2. \quad (3.10)$$

The twist-2 operator does not contribute at LO.

4. Dark Matter Direct Detection at One-Loop Order

Let us now calculate the NLO electroweak (EW) contribution to the cross section. Here again we will just briefly review our calculation in [13] and present some updates to the calculation. We need to determine the Wilson coefficients f_q and f_G related to the operators in Eq. (3.2). At NLO EW also g_q contributes to the cross section. The diagrams contributing at NLO EW are shown in Fig. 3.

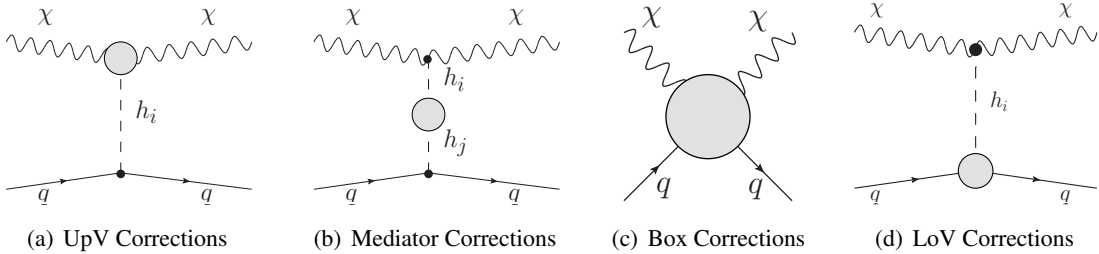


Figure 3: Generic one-loop corrections to the scattering of VDM with the nucleon. The grey blob corresponds to the renormalized one-loop corrections. The corrections can be separated into upper vertex (a), mediator (b), box (c) and lower vertex (d) corrections.

In our study presented in [13] we have not included the contributions of the diagrams in Fig. 3(d). These were now included and the results presented here are updated. The treatment of the diagrams will be discussed in detail in Sec. 4.5.

4.1 Upper Vertex Corrections $\chi\chi h_i$

The effective one-loop coupling $\chi\chi h_i$ is extracted from the loop corrections to the $\chi\chi h_i$ coupling. We take the DM particles on-shell and assume $p_{h_i} = 0$. The amplitude for the NLO vertex (in this section we will refer to the upper vertex as just the vertex) can be written as

$$i\mathcal{A}_{\chi\chi h_i}^{\text{NLO}} = i\mathcal{A}_{\chi\chi h_i}^{\text{LO}} + i\mathcal{A}_{\chi\chi h_i}^{\text{VC}} + i\mathcal{A}_{\chi\chi h_i}^{\text{CT}}, \quad (4.1)$$

where $i\mathcal{A}_{\chi\chi h_i}^{\text{LO}}$ is the LO contribution, $i\mathcal{A}_{\chi\chi h_i}^{\text{VC}}$ are the virtual vertex corrections and $i\mathcal{A}_{\chi\chi h_i}^{\text{CT}}$ are the counterterms contributions. The LO amplitude is

$$i\mathcal{A}_{\chi\chi h_i}^{\text{LO}} = g_{\chi\chi h_i} \varepsilon(p) \cdot \varepsilon^*(p) = 2g_{\chi} m_{\chi} \varepsilon(p) \cdot \varepsilon^*(p) \begin{cases} \sin \alpha, & i = 1 \\ \cos \alpha, & i = 2 \end{cases}, \quad (4.2)$$

where p denotes the four-momentum of the incoming VDM particle and ε its polarization vector. The vertex counterterm amplitudes for $i = 1, 2$ are

$$i\mathcal{A}_{\chi \rightarrow \chi h_1}^{\text{CT}} = \left[\frac{1}{2} (g_{\chi\chi h_2} \delta Z_{h_2 h_1} + g_{\chi\chi h_1} \delta Z_{h_1 h_1}) + g_{\chi\chi h_1} \delta Z_{\chi\chi} + \delta g_{\chi\chi h_1} \right] \varepsilon(p) \cdot \varepsilon^*(p) \quad (4.3a)$$

$$i\mathcal{A}_{\chi \rightarrow \chi h_2}^{\text{CT}} = \left[\frac{1}{2} (g_{\chi\chi h_1} \delta Z_{h_1 h_2} + g_{\chi\chi h_2} \delta Z_{h_2 h_2}) + g_{\chi\chi h_2} \delta Z_{\chi\chi} + \delta g_{\chi\chi h_2} \right] \varepsilon(p) \cdot \varepsilon^*(p), \quad (4.3b)$$

with the counterterms $\delta g_{\chi\chi h_i}$ ($i = 1, 2$) for the respective tree-level couplings

$$g_{\chi\chi h_1} = 2g_{\chi} m_{\chi} \sin \alpha \quad (4.4)$$

$$g_{\chi\chi h_2} = 2g_{\chi} m_{\chi} \cos \alpha \quad (4.5)$$

derived from

$$\delta g_{\chi\chi h_i} = \sum_p \frac{\partial g_{\chi\chi h_i}}{\partial p} \delta p, \quad p \in \{m_{\chi}^2, g_{\chi}, \alpha\}. \quad (4.6)$$

At NLO two additional tensor structures arise

$$i\mathcal{A}^{\text{NLO}} = (\dots) \underbrace{\varepsilon(p_{\text{in}}) \cdot \varepsilon^*(p_{\text{out}})}_{\sim \text{LO}} + (\dots) \underbrace{(p_{\text{in}} \cdot \varepsilon^*(p_{\text{out}})) (p_{\text{out}} \cdot \varepsilon(p_{\text{in}}))}_{\sim \text{NLO}}, \quad (4.7)$$

where p_{in} (p_{out}) is the incoming (outgoing) momentum of the DM vector gauge boson. The additional new tensor structure (denoted by $\sim \text{NLO}$) vanishes by assuming $p_{\text{in}} = p_{\text{out}}$ implying $\varepsilon(p) \cdot p = 0$. As for the amplitude that corrects the LO contribution we have checked that it is UV finite. The amplitude is then projected onto the corresponding tensor structure, the vertex corrections are plugged in the generic diagram in Fig. 3(a) which contributes to the operator $\chi_{\mu} \chi^{\mu} m_q \bar{q} q$. This contribution is referred to as f_q^{vertex} .

4.2 Mediator Corrections

For the mediator correction one takes the self-energy corrections to the two-point functions with all external Higgs fields and inserts them in the one-loop propagator in the generic amplitude in Fig. 3(b). The self-energy contribution to the $h_i h_j$ propagator ($i, j = 1, 2$) reads

$$\Delta_{h_i h_j} = - \frac{\hat{\Sigma}_{h_i h_j}(p^2 = 0)}{m_{h_i}^2 m_{h_j}^2}, \quad (4.8)$$

with the renormalised self-energy matrix

$$\begin{pmatrix} \hat{\Sigma}_{h_1 h_1} & \hat{\Sigma}_{h_1 h_2} \\ \hat{\Sigma}_{h_2 h_1} & \hat{\Sigma}_{h_2 h_2} \end{pmatrix} \equiv \hat{\Sigma}(p^2) = \Sigma(p^2) - \delta m^2 - \delta T + \frac{\delta Z}{2} (p^2 - \mathcal{M}^2) + (p^2 - \mathcal{M}^2) \frac{\delta Z}{2}, \quad (4.9)$$

where the mass matrix \mathcal{M} and the tadpole counterterm matrix δT are defined in Eq. (2.27). The Z-factor matrix δZ corresponds to the matrix with the components $\delta Z_{h_i h_j}$ defined in Eq. (2.33). Projecting the resulting one-loop correction on the corresponding tensor structure, we get the one-loop correction to the Wilson coefficient of the operator $\chi_\mu \chi^\mu m_q \bar{q} q$

$$f_q^{\text{med}} = \frac{gg\chi m_\chi}{2m_W} \sum_{i,j} R_{\alpha,i2} R_{\alpha,j1} \Delta_{h_i h_j}, \quad (4.10)$$

with the rotation matrix R_α defined in Eq. (2.8).

4.3 Box Corrections

In the following we want to present the treatment of the box diagrams contributing to the SI cross section. The relevant terms of the box diagram tensor structures in the spin-independent cross section are extracted using an expansion in the loop diagrams. This expansion is performed in terms of the non-relativistic momentum p_q of the external quark [11]. The box diagrams contribute to $X_\mu X^\mu m_q \bar{q} q$ and the twist-2 operators which becomes clear if we write [12, 50, 51]

$$\bar{q} i \partial_\mu \gamma_\nu q = \mathcal{O}_{\mu\nu}^q + \bar{q} \frac{i \partial_\mu \gamma_\nu - i \partial_\nu \gamma_\mu}{2} q + \frac{1}{4} g_{\mu\nu} m_q \bar{q} q, \quad (4.11)$$

where the asymmetric part in Eq. (4.11) does not contribute to the SI cross section. We will refer to these one-loop contributions to the corresponding tree-level Wilson coefficients as f_q^{box} and g_q^{box} .

There are still contributions from the effective gluon interaction with the DM particles that will contribute to the Wilson coefficient f_G in Eq. (3.2b). As shown in [11] the use of Eq. (3.7) to obtain the gluon interaction induces large errors. An ansatz was proposed in Ref. [12] for heavy quarks compared to the mediator mass, by deriving an effective coupling between two Higgs bosons and the gluon fields. Integrating out the top-quark leads to the effective two-Higgs-two-gluon coupling [12]

$$\mathcal{L}^{hhGG} = \frac{1}{2} d_G^{\text{eff}} h_i h_j \frac{\alpha_S}{12\pi} G_{\mu\nu}^a G^{a\mu\nu}, \quad (4.12)$$

with

$$d_G^{\text{eff}} \rightarrow (d_G^{\text{eff}})_{ij} = (R_\alpha)_{i1} (R_\alpha)_{j1} \frac{1}{v^2}. \quad (4.13)$$

We note that In Ref. [12], the full two-loop calculation was performed showing very good agreement with the approximate result for mediator masses below m_t . Moreover, the box contribution to the NLO SI direct detection cross section is several orders of magnitude below the LO contribution as we will show later.

The diagram in Fig. 4 (right) yields the following contribution to the Lagrangian

$$\mathcal{L}_{\text{eff}} \supset (d_G^{\text{eff}})_{ij} C_\Delta^{ij} \chi_\mu \chi^\mu \frac{-\alpha_S}{12\pi} G_{\mu\nu}^a G^{a\mu\nu}, \quad (4.14)$$

where C_Δ^{ij} denotes the contribution from the triangle loop built up by h_i , h_j and the VDM particle. It has to be extracted from the calculated amplitude of Fig. 4 (right). Using Eq. (3.2b) the contributions by the box topology to the gluon-DM interaction is given by

$$f_G^{\text{top}} = (d_G^{\text{eff}})_{ij} C_\Delta^{ij} \frac{-\alpha_S}{12\pi}. \quad (4.15)$$

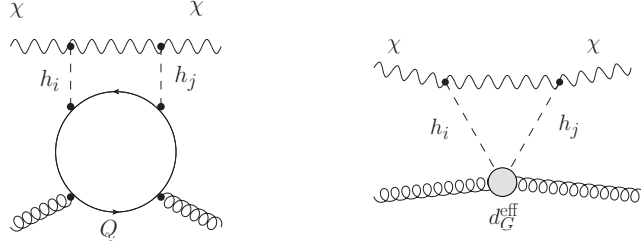


Figure 4: The full two-loop gluon interaction with the DM candidate (left) and the effective two-loop interaction after integration out the heavy quarks (right).

4.4 The SI One-Loop Cross Section

We can now write the NLO EW SI cross section using the effective one-loop form factor

$$\frac{f_N^{\text{NLO}}}{m_N} = \sum_{q=u,d,s} f_q^{\text{NLO}} f_{T_q}^N + \sum_{q=u,d,s,c,b} \frac{3}{4} (q(2) + \bar{q}(2)) g_q^{\text{NLO}} - \frac{8\pi}{9\alpha_S} f_{T_G}^N f_G^{\text{NLO}}, \quad (4.16)$$

with the Wilson coefficients at one-loop level given by

$$f_q^{\text{NLO}} = f_q^{\text{vertex}} + f_q^{\text{med}} + f_q^{\text{box}} \quad (4.17a)$$

$$g_q^{\text{NLO}} = g_q^{\text{box}} \quad (4.17b)$$

$$f_G^{\text{NLO}} = -\frac{\alpha_S}{12\pi} \sum_{q=c,b,t} (f_q^{\text{vertex}} + f_q^{\text{med}}) + f_G^{\text{top}}. \quad (4.17c)$$

Like at LO, the heavy quark contributions of f_q^{vertex} and f_q^{med} have to be attributed to the effective gluon interaction. With the LO form factor given by

$$\frac{f_N^{\text{LO}}}{m_N} = f_q^{\text{LO}} \left[\sum_{q=u,d,s} f_{T_q}^N + \sum_{q=c,b,t} \frac{2}{27} f_{T_G}^N \right], \quad (4.18)$$

where f_q^{LO} has been given in Eq. (3.8), we have for the NLO EW SI cross section at leading order in α_S ,

$$\sigma_N = \frac{1}{\pi} \left(\frac{m_N}{m_\chi + m_N} \right)^2 [|f_N^{\text{LO}}|^2 + 2\text{Re}(f_N^{\text{LO}} f_N^{\text{NLO}*})]. \quad (4.19)$$

4.5 The inclusion of the lower vertex corrections

In our approach in [13] we have neglected the EW corrections of the lower vertex $q\bar{q}h_i$ due to the missing cancellation of IR divergencies. This naive approach gives rise to several subtle problems to be discussed in the following. The field strength renormalisation constants $\delta Z_{h_i h_j}$ in Eq. (2.33) for the Higgs boson mediator are introduced artificially. Considering the full process these *internal* field strength renormalisation constants (referred to as $\mathcal{A}_i^{\delta Z}$) would cancel exactly

$$\left(\mathcal{A}_{upV}^{\text{VC}} + \mathcal{A}_{upV}^{\text{gCT}} \right) + \left(\mathcal{A}_{med}^{\text{VC}} + \mathcal{A}_{med}^{\text{gCT}} \right) + \left(\mathcal{A}_{LV}^{\text{VC}} + \mathcal{A}_{LV}^{\text{gCT}} \right) + \underbrace{\mathcal{A}_{upV}^{\delta Z} + \mathcal{A}_{med}^{\delta Z} + \mathcal{A}_{LV}^{\delta Z}}_{=0} = \text{UV finite}, \quad (4.20)$$

where $\mathcal{A}_i^{\text{VC}}$ corresponds to the genuine one-loop diagrams and $\mathcal{A}_i^{\text{gCT}}$ to the counterterm amplitude (without the $\delta Z_{h_i h_j}$ factor). The box contributions are not relevant for the problem and therefore dropped in the following discussion. The contributions of the upper vertex $\chi\chi h_i$ are referred to as UpV , the lower vertex $q\bar{q}h_i$ as LoV and mediator corrections as med , respectively. The artificial introduction of the δZ part allows to cancel the UV-poles topology-wise

$$\left(\mathcal{A}_i^{\text{VC}} + \mathcal{A}_i^{\text{gCT}}\right)_{\text{fin.}} + \underbrace{\left(\mathcal{A}_i^{\text{VC}} + \mathcal{A}_i^{\text{gCT}}\right)_{\Delta}}_{=0} + \left(\mathcal{A}_i^{\delta Z}\right)_{\Delta} + \left(\mathcal{A}_i^{\delta Z}\right)_{\text{fin.}}, \quad (i = UpV, LoV, med), \quad (4.21)$$

where $(\dots)_{\Delta}$ indicates the explicit UV pole of the amplitude and $(\dots)_{\text{fin.}}$ the finite part, respectively. By dropping the full lower vertex in the matching of the Wilson coefficients the finite piece $-\mathcal{A}_{LV}^{\delta Z}$ would remain in the amplitude due to the missing cancellation indicated in Eq. (4.20).

As an additional issue, the chosen renormalisation scheme for the mixing angle $\delta\alpha$ was shown [43, 53] to be numerically stable only if either $\delta\alpha$ and $\delta Z_{h_i h_j}$ occur in a specific combination, or by including *all diagrams* of the process yielding a numerically stable combination of $\delta\alpha$. The former case is present in on-shell decays and the latter is our present approach. This numerical instability is related to the $\frac{1}{m_{h_1}^2 - m_{h_2}^2}$ mass pole used in the definition of the mixing angle. Note that this pole also occurs explicitly in the off-diagonal $\delta Z_{h_i h_j}$ field strength renormalisation constants of the Higgs bosons. By dropping the lower vertex the cancellation of the mass pole due to the mixing angle counterterm combination would also not be present anymore and the result would be numerically unstable. Note that by stability we mean that the numbers are not unnaturally large.

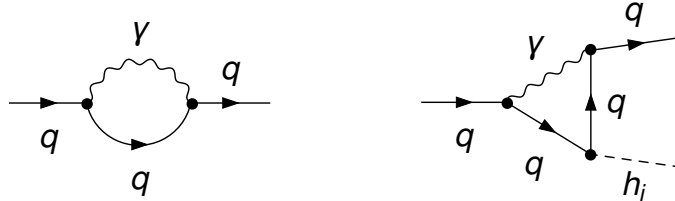


Figure 5: QED subset contribution to the lower vertex coefficient. The QED subset is UV finite and contains all IR divergences.

By artificially including the $\delta Z_{h_i h_j}$ in the mediator counterterm and dropping the lower vertex as proposed in [13], the Higgs mediator is treated as *on shell* so that the mass pole $1/m_h^2 - m_\phi^2$ of the δZ remainder ($-\mathcal{A}_{LV}^{\delta Z}$ in Eq. (4.20)) and the $\delta\alpha$ mass pole remainder of the upper vertex cancel each other exactly. In this way numerically stable EW NLO corrections could be obtained. However, this cancellation is unphysical and should be avoided, indicating that the dropping of the lower vertex is not the optimal solution.

The IR divergent diagrams of the lower vertex, shown in Fig. 5, form a UV-finite subset, referred to as QED subset in the following. This QED subset includes all lower vertex corrections and quark self-energies containing a photon line. Expanding this QED subset for strictly vanishing external quark momentum and neglecting all terms of the order $\mathcal{O}(p_Q^2)$ which is also compatible

with the expansion used in the box calculation in [13], allows to regulate all IR divergencies. In this way the lower vertex, which is a sum of all contributions without a photon and the QED subset, is explicitly UV finite and all IR divergencies are regulated by the strict vanishing quark momentum expansion. Using the expansion allows to include the lower vertex in the matching of the Wilson coefficients without including any IR divergences and thereby the cancellation of Eq. (4.20) is present. The unphysical treatment of the internal Higgs mediator is avoided and a numerically stable result is obtained.

The inclusion of the EW corrections to the lower vertex, however, invalidate the replacement rule of Eq. (3.7) for the lower vertex. So far the QCD trace anomaly is calculated at one-loop (QCD) level to find the relation between the heavy quark operator $m_Q \bar{Q}Q$ ($Q = c, b, t$) and gluon field-strength operator $G_a^{\mu\nu} G^{a,\mu\nu}$. Including EW corrections spoil this replacement rule and the proper matching is beyond the scope of this analysis. Therefore, the EW corrections of the lower vertex with a heavy quark cannot be considered in the calculation of the gluon contribution to the spin-independent cross section, since otherwise the cancellation of Eq. (4.20) would fail again. Hence, the DM-gluon interaction is determined only considering EW LO diagrams and using the replacement rule Eq. (3.7). In this way the problem discussed above with the $\delta Z_{h_i, h_j}$ is avoided.

5. Numerical Analysis

The VDM model was implemented in the `ScannerS` [54, 55] code which automatizes the parameter scan. The points generated are constrained by

- The SM-like Higgs boson has a mass of $m_h = 125.09$ GeV [56].
- The potential is in a global minimum and all points satisfy the theoretical constraints of boundedness from below and perturbative unitarity. We furthermore impose the perturbativity constraint $g_\chi^2 < 4\pi$.
- The mixing angle α is constrained by the combined values for the signal strengths [56]. An interface with `HiggsBounds` [57–59] allows to check for collider bounds from LEP, Tevatron and the LHC. We require agreement with the exclusion limits derived for the non-SM-like Higgs boson at 95% confidence level. The most stringent bound arises from searches for heavy ZZ resonances [60].
- Calculations of the Higgs decay widths and branching ratios are performed with `SHDECAY` [55]², which includes the state-of-the-art higher-order QCD corrections. The code `SHDECAY` is based on the implementation of the models in `HDECAY` [61, 62].
- Information on the DM particle is taken into account from LHC searches through the invisible width of the SM Higgs boson [57–59].
- The DM relic abundance was calculated with `MicrOmEGAs` [63–66], and compared with the current experimental result from the Planck Collaboration [67],

$$(\Omega h^2)_{\text{DM}}^{\text{obs}} = 0.1186 \pm 0.002 . \quad (5.1)$$

²The program `SHDECAY` can be downloaded from the url: <http://www.itp.kit.edu/~maggie/SHDECAY>.

| | m_ϕ [GeV] | m_χ [GeV] | v_S [GeV] | α |
|-----|----------------|----------------|-------------|------------------|
| min | 1 | 1 | 1 | $-\frac{\pi}{4}$ |
| max | 1000 | 1000 | 10^7 | $\frac{\pi}{4}$ |

Table 1: Input parameters for the VDM model scan, all parameters varied independently between the given minimum and maximum values. The SM-like Higgs boson mass is set $m_h = 125.09$ GeV and the SM VEV $v = 246.22$ GeV.

We require the calculated abundance to be equal to or smaller than the observed one, that is, we allow the DM not to saturate the relic density and therefore define a DM fraction

$$f_{\chi\chi} = \frac{(\Omega h^2)_\chi}{(\Omega h^2)_{\text{DM}}^{\text{obs}}}, \quad (5.2)$$

where $(\Omega h^2)_\chi$ stands for the calculated DM relic abundance of the VDM model.

- DM indirect detection does not play a relevant role here. See [13] for details.
- The sample was generated taking into account the direct detection bound on the DM nucleon SI cross section at LO. The most stringent experimental bound is the one from the XENON1T [68,69] experiment. We apply the latest XENON1T upper bounds [69] for a DM mass above 6 GeV and the combined limits from CRESST-II [70] and CDMSlite [71] are used for lighter DM particles. Because the experimental limits on the DM-nucleon scattering assume the DM candidate to make up for all of the DM abundance, the correct quantity to be compared with the experimental limits is the effective DM-nucleon cross-section defined by

$$\sigma_{\chi N}^{\text{eff}} \equiv f_{\chi\chi} \sigma_{\chi N}, \quad (5.3)$$

where χN stands for the scattering of the VDM particle χ with the nucleon N , and $f_{\chi\chi}$ denotes the respective DM fraction, defined in Eq. (5.2). In our numerical analysis, we use the LO and NLO results for $N = p$.

The ranges of the input parameters for the scan are shown in Table 1. From now on we denote the non-SM like Higgs boson mass as m_ϕ and the SM-like Higgs boson mass as m_h . The remaining input parameters, gauge, lepton and quark masses, electric coupling, Weinberg angle and weak $SU(2)$ coupling, are set to

$$\begin{aligned} m_W &= 80.398 \text{ GeV} , & m_Z &= 91.1876 \text{ GeV} , & \sin \theta_W &= 0.4719 , \\ m_e &= 0.511 \cdot 10^{-3} \text{ GeV} , & m_\mu &= 0.1057 \text{ GeV} , & m_\tau &= 1.777 \text{ GeV} , \\ m_u &= 0.19 \text{ MeV} , & m_d &= 0.19 \text{ MeV} , & m_s &= 0.19 \text{ MeV} , \\ m_c &= 1.4 \text{ GeV} , & m_b &= 4.75 \text{ GeV} , & m_t &= 172.5 \text{ GeV} . \end{aligned} \quad (5.4)$$

For the proton mass we take

$$m_p = 0.93827 \text{ GeV} . \quad (5.5)$$

6. Results

We will now present the results with the NLO corrections, focusing on the main changes relative to our previous work [13]. The sample used complies with all theoretical and experimental bounds described in the previous section. We note that the bound for direct detection at LO is already imposed and that, in order to be able to compare with the Xenon limit, we applied the correction factor $f_{\chi\chi}$ to the LO and NLO direct detection cross section, *cf.* Eq. (5.3).

6.1 Relative size of one-loop corrections

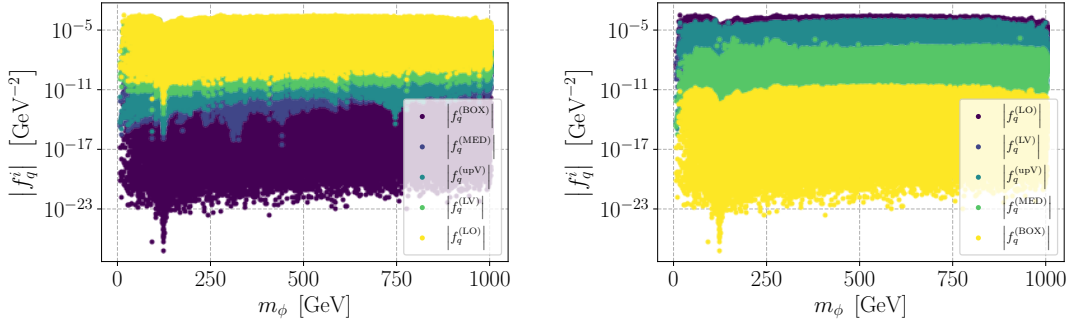


Figure 6: we need units on the y axis which I believe are $[\sigma]/[m]$

Value of the Wilson coefficients of the different NLO contributions as compared to the LO, with the LO colour on top (left) and reversed colour code (right).

In Fig. 6 we present the values of the Wilson coefficients contributing to the LO and to the NLO cross sections with the colour code where the largest contributions are on top (on the left) and the inverted colour code (on the right) as a function of the non-SM-like Higgs boson mass m_ϕ . The order of the relevance of the contributions is clear from the two plots. The LO is about one order of magnitude above the most relevant one-loop corrections which are the vertex contribution, both the lower and upper one. Another clear point revealed by the plots is that the box contributions are several orders of magnitude below the vertex corrections and are therefore negligible. In Fig. 7 we

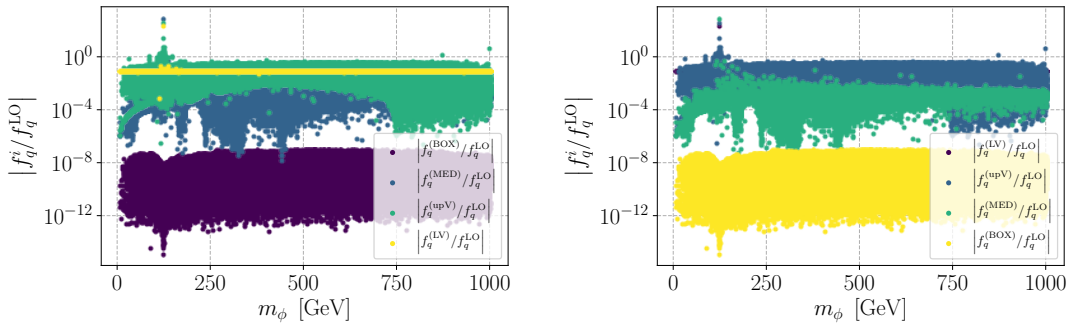


Figure 7: Value of the Wilson coefficients of the different NLO contributions, normalised to the LO coefficient, with the LO colour on top (left) and reversed colour code (right).

present the same NLO Wilson coefficients but now normalised to the LO result and the same colour

code as a function of the non-SM-like Higgs boson mass m_ϕ . In this plot the relative importance of the lower and the upper vertex becomes clearer from the plot on the left. The right plot shows that the mediator contribution also plays a role in particular close to the SM Higgs boson mass. Again, box contributions are clearly negligible.

6.2 K -factors and Impact of the NLO Corrections on the Xenon Limit

We now turn to the comparison of the NLO to the LO cross section of direct detection. In Fig. 8 we show the K -factor, *i.e.* the ratio between NLO and LO cross section, as a function of the LO SI direct detection cross section (left) and as a function of the non-SM-like Higgs boson mass m_ϕ (right). The size of g_χ is indicated by the color code. The main points to note are the following: the K -factor increases with g_χ but except for the outliers the increase is always below about 30%; the outliers, clearly seen on the right plot, appear close to $m_\phi = m_h$ with K -factors close to 2 which are due to the resonant behaviour in the vertex contributions. The values for the K -factors are much smaller than the ones obtained in our previous study [13] where we could see K -factors reaching 100%. This is the main difference we found after the inclusion of the lower vertex contribution. Also the resonant contributions are more stable with values of K -factors below about 2. The K -

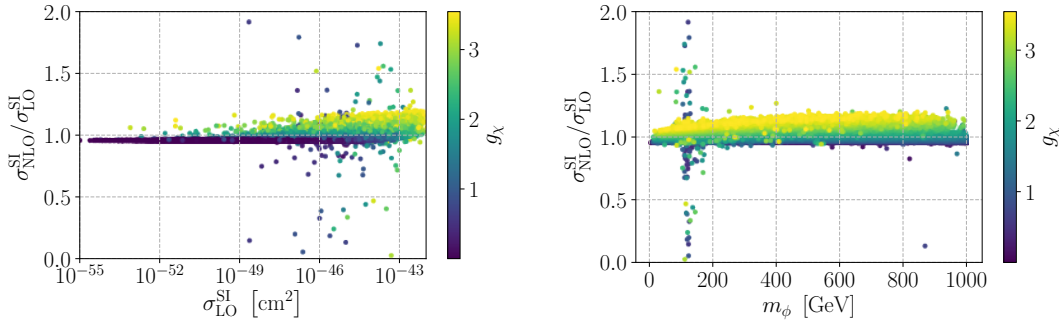


Figure 8: K -factor as function of the LO direct detection cross section (left) and as a function of the non-125 GeV Higgs mass (right). The color code denotes the size of the dark gauge coupling g_χ .

factor shows no particularly interesting dependence on the other free parameters, the mixing angle α and the vector DM mass.

Both the LO and the NLO contributions to the SI direct detection cross section are proportional to the LO amplitude and are therefore proportional to $\sin 2\alpha$ and $m_h^2 - m_\chi^2$. Hence, blind spots are the same at LO and at NLO. In our scan we did not find any other points where a specific parameter combination would lead to an accidental suppression at LO that is removed at NLO. The blind spot at $\alpha = 0$ represents a scenario where the SM-like Higgs boson has exactly SM-like couplings and the new scalar only couples to the Higgs and to dark matter. The SM-like Higgs decouples from dark matter and we may end up with two dark matter candidates with the second scalar being metastable.

We end this section with a discussion of the phenomenological impact of our NLO results on the Xenon limit. In Fig. 9 we show the allowed parameter space in the (m_ϕ, m_χ) plane with all constraints taken into account. The blue points are the ones valid for the LO direct detection cross section. In the left plot the green points are the ones excluded at NLO and in the right plot they

represent the allowed points at NLO. The plots tell us that although we see a very large number of points excluded at NLO, the difference between LO and NLO would hardly be seen in a scan.

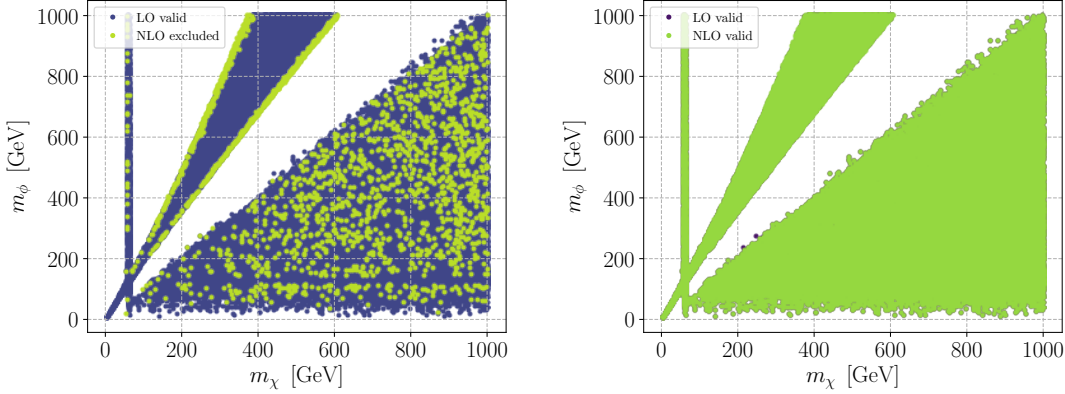


Figure 9: The SI cross section including the correction factor $f_{\chi\chi}$ at LO (blue) and NLO (orange) compared to the Xenon limit (blue-dashed) versus the DM mass m_χ . The definition of the parameter sample included in the left and right plots is described in the text.

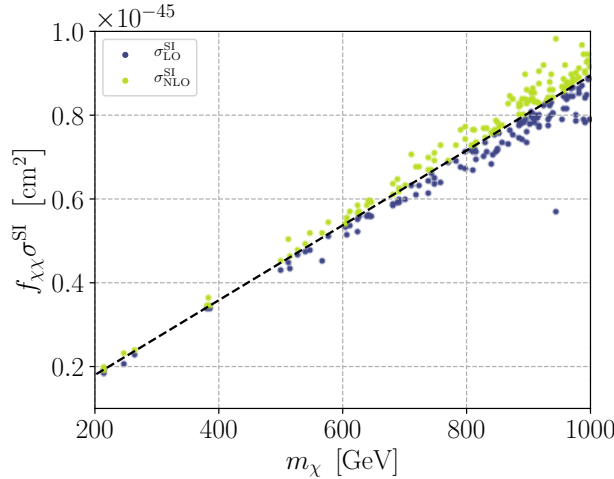


Figure 10: The SI cross section including the correction factor $f_{\chi\chi}$ at LO (blue) and NLO (green) compared to the Xenon limit (blue-dashed) versus the DM mass m_χ .

In order to understand the difference between LO and NLO at the phenomenological level we present in Fig. 10 the SI cross section including the correction factor $f_{\chi\chi}$ at LO (blue) and NLO (green) compared to the Xenon limit (blue-dashed) versus the DM mass m_χ . In this plot we show all parameter points where the LO cross section does not exceed the Xenon limit but the NLO result does. Clearly, there is a sizeable number of parameter points where compatibility with the experimental constraints at NLO would no longer hold. Therefore, NLO corrections need to be accounted for in order to make reliable predictions about the viable parameter space of the VDM model. It can also be that for some parameter points for which the LO cross section is much smaller

than the Xenon limit, the NLO cross section is of the order of the Xenon limit. In this case, although LO results might suggest that the Xenon experiment is not sensitive to the model, this is no longer true when NLO corrections are taken into account. These results confirm the importance of the NLO corrections when interpreting the data.

7. Conclusions

This paper is an update to a previous work [13] where we have computed the NLO corrections to the SI direct detection cross section for the scattering of the VDM particle off a nucleon. This minimal model is an extension of the SM with a vector dark matter particle and a new scalar that mixes with the SM Higgs. Relative to our previous work we have included the contribution of the NLO corrections to the lower vertex, that is, the qgh vertex. This was possible after we have devised a way to treat the IR divergences that appear in these corrections.

The overall conclusions are the same but the results are somewhat more stable with the K -factor for NLO corrections being slightly smaller. There is clear hierarchy in the significance of the NLO corrections where the leading role belongs to both vertex corrections followed by mediator and finally by the box corrections. The interference effects between the two scalar particles, relevant for degenerate mass values, were again found to be large and require further investigations beyond the scope of this paper. Outside this region, the perturbative series is well-behaved.

From the phenomenological point of view the overall conclusions are again the same. The NLO corrections can increase the LO results to values where the Xenon experiment becomes sensitive to the model, or to values where the model is even excluded due to cross sections above the Xenon limit. In case of suppression, parameter points that might be rejected at LO may render the model viable when NLO corrections are included.

Acknowledgments

We are thankful to M. Gabelmann, M. Krause and M. Spira for fruitful and clarifying discussions. We are grateful to D. Azevedo for providing us with the data samples. R.S. is supported by the Portuguese Foundation for Science and Technology (FCT), Contracts UIDB/00618/2020, UIDP/00618/2020, PTDC/FIS-PAR/31000/2017 and CERN/FISPAR/0002/2017, and by the HARMONIA project, contract UMO-2015/18/M/S. The work of MM is supported by the BMBF-Project 05H18VKCC1, project number 05H2018.

A. Nuclear Form Factors

We here present the numerical values for the nuclear form factors defined in Eq. (3.4). The values of the form factors for light quarks are taken from `micrOmegas` [72]

$$f_{T_u}^p = 0.01513, \quad f_{T_d}^p = 0.00191, \quad f_{T_s}^p = 0.0447, \quad (\text{A.1a})$$

$$f_{T_u}^n = 0.0110, \quad f_{T_d}^n = 0.0273, \quad f_{T_s}^n = 0.0447, \quad (\text{A.1b})$$

which can be related to the gluon form factors as

$$f_{T_G}^p = 1 - \sum_{q=u,d,s} f_{T_q}^p, \quad f_{T_G}^n = 1 - \sum_{q=u,d,s} f_{T_q}^n. \quad (\text{A.2})$$

The needed second momenta in Eq. (3.4) are defined at the scale $\mu = m_Z$ by using the CTEQ parton distribution functions [73],

$$u^p(2) = 0.22, \quad \bar{u}^p(2) = 0.034, \quad (\text{A.3a})$$

$$d^p(2) = 0.11, \quad \bar{d}^p(2) = 0.036, \quad (\text{A.3b})$$

$$s^p(2) = 0.026, \quad \bar{s}^p(2) = 0.026, \quad (\text{A.3c})$$

$$c^p(2) = 0.019, \quad \bar{c}^p(2) = 0.019, \quad (\text{A.3d})$$

$$b^p(2) = 0.012, \quad \bar{b}^p(2) = 0.012, \quad (\text{A.3e})$$

where the respective second momenta for the neutron can be obtained by interchanging up- and down-quark values.

References

- [1] F. Zwicky, *Helv. Phys. Acta* **6**, 110 (1933), [*Gen. Rel. Grav.*41,207(2009)].
- [2] M. W. Goodman and E. Witten, *Phys. Rev.* **D31**, 3059 (1985), [,325(1984)].
- [3] U. Haisch and F. Kahlhoefer, *JCAP* **1304**, 050 (2013), 1302.4454.
- [4] A. Crivellin, F. D’Eramo, and M. Procura, *Phys. Rev. Lett.* **112**, 191304 (2014), 1402.1173.
- [5] R. J. Hill and M. P. Solon, *Phys. Rev.* **D91**, 043504 (2015), 1401.3339.
- [6] T. Abe and R. Sato, *JHEP* **03**, 109 (2015), 1501.04161.
- [7] M. Klasen, K. Kovarik, and P. Steppeler, *Phys. Rev.* **D94**, 095002 (2016), 1607.06396.
- [8] D. Azevedo *et al.*, *JHEP* **01**, 138 (2019), 1810.06105.
- [9] K. Ishiwata and T. Toma, *JHEP* **12**, 089 (2018), 1810.08139.
- [10] K. Ghorbani and P. H. Ghorbani, *JHEP* **05**, 096 (2019), 1812.04092.
- [11] T. Abe, M. Fujiwara, and J. Hisano, *JHEP* **02**, 028 (2019), 1810.01039.
- [12] F. Ertas and F. Kahlhoefer, *JHEP* **06** (2019), 052 [arXiv:1902.11070 [hep-ph]].
- [13] S. Glaus, M. Mühlleitner, J. Müller, S. Patel and R. Santos, *JHEP* **10** (2019), 152, 1908.09249.
- [14] T. Hambye, *JHEP* **01**, 028 (2009), 0811.0172.
- [15] O. Lebedev, H. M. Lee, and Y. Mambrini, *Phys. Lett.* **B707**, 570 (2012), 1111.4482.
- [16] Y. Farzan and A. R. Akbarieh, *JCAP* **1210**, 026 (2012), 1207.4272.
- [17] S. Baek, P. Ko, W.-I. Park, and E. Senaha, *JHEP* **05**, 036 (2013), 1212.2131.
- [18] S. Baek, P. Ko, and W.-I. Park, *Phys. Rev.* **D90**, 055014 (2014), 1405.3530.
- [19] M. Duch, B. Grzadkowski, and M. McGarrie, *JHEP* **09**, 162 (2015), 1506.08805.
- [20] D. Azevedo *et al.*, *Phys. Rev.* **D99**, 015017 (2019), 1808.01598.

- [21] S. Yaser Ayazi, and A. Mohamadnejad, *JHEP* **03**, (2019) 181, 1901.04168.
- [22] T. Hahn, *Comput. Phys. Commun.* **140**, 418 (2001), hep-ph/0012260.
- [23] F. Staub, *Comput. Phys. Commun.* **185**, 1773 (2014), 1309.7223.
- [24] F. Staub, *Comput. Phys. Commun.* **184**, 1792 (2013), 1207.0906.
- [25] F. Staub, *Comput. Phys. Commun.* **182**, 808 (2011), 1002.0840.
- [26] F. Staub, *Comput. Phys. Commun.* **181**, 1077 (2010), 0909.2863.
- [27] V. Shtabovenko, R. Mertig, and F. Orellana, *Comput. Phys. Commun.* **207**, 432 (2016), 1601.01167.
- [28] R. Mertig, M. Bohm, and A. Denner, *Comput. Phys. Commun.* **64**, 345 (1991).
- [29] T. Hahn and M. Perez-Victoria, *Comput. Phys. Commun.* **118** (1999), 153-165
doi:10.1016/S0010-4655(98)00173-8 [arXiv:hep-ph/9807565 [hep-ph]].
- [30] G. Passarino and M. J. G. Veltman, *Nucl. Phys.* **B160**, 151 (1979).
- [31] A. Denner, S. Dittmaier, and L. Hofer, *Comput. Phys. Commun.* **212**, 220 (2017), 1604.06792.
- [32] A. Denner and S. Dittmaier, *Nucl. Phys.* **B658**, 175 (2003), hep-ph/0212259.
- [33] A. Denner and S. Dittmaier, *Nucl. Phys.* **B734**, 62 (2006), hep-ph/0509141.
- [34] A. Denner and S. Dittmaier, *Nucl. Phys.* **B844**, 199 (2011), 1005.2076.
- [35] M. Krause, R. Lorenz, M. Muhlleitner, R. Santos, and H. Ziesche, *JHEP* **09**, 143 (2016), 1605.04853.
- [36] F. Bojarski, G. Chalons, D. Lopez-Val, and T. Robens, *JHEP* **02**, 147 (2016), 1511.08120.
- [37] A. Denner, L. Jenniches, J.-N. Lang, and C. Sturm, *JHEP* **09**, 115 (2016), 1607.07352.
- [38] M. Krause, M. Muhlleitner, R. Santos, and H. Ziesche, *Phys. Rev.* **D95**, 075019 (2017), 1609.04185.
- [39] M. Krause, D. Lopez-Val, M. Muhlleitner, and R. Santos, *JHEP* **12**, 077 (2017), 1708.01578.
- [40] L. Altenkamp, S. Dittmaier, and H. Rzehak, *JHEP* **09**, 134 (2017), 1704.02645.
- [41] L. Altenkamp, S. Dittmaier, and H. Rzehak, *JHEP* **03**, 110 (2018), 1710.07598.
- [42] M. Fox, W. Grimus, and M. Löschner, *Int. J. Mod. Phys.* **A33**, 1850019 (2018), 1705.09589.
- [43] A. Denner, S. Dittmaier and J. N. Lang, *JHEP* **11** (2018), 104 doi:10.1007/JHEP11(2018)104 [arXiv:1808.03466 [hep-ph]].
- [44] W. Grimus and M. Löschner, (2018), 1807.00725.
- [45] M. Krause, M. Mühlleitner, and M. Spira, (2018), 1810.00768.
- [46] M. Krause and M. Mühlleitner, (2019), 1904.02103.
- [47] A. Pilaftsis, *Nucl. Phys.* **B504**, 61 (1997), hep-ph/9702393.
- [48] S. Kanemura, Y. Okada, E. Senaha, and C. P. Yuan, *Phys. Rev.* **D70**, 115002 (2004), hep-ph/0408364.
- [49] J. Hisano, K. Ishiwata, N. Nagata, and M. Yamanaka, *Prog. Theor. Phys.* **126**, 435 (2011), 1012.5455.
- [50] J. Hisano, K. Ishiwata, and N. Nagata, *Phys. Rev.* **D82**, 115007 (2010), 1007.2601.

- [51] J. Hisano, R. Nagai, and N. Nagata, *JHEP* **05**, 037 (2015), 1502.02244.
- [52] M. A. Shifman, A. I. Vainshtein, and V. I. Zakharov, *Phys. Lett.* **78B**, 443 (1978).
- [53] A. Denner, S. Dittmaier and J. N. Lang, doi:10.22323/1.375.0076 [arXiv:1912.02425 [hep-ph]].
- [54] R. Coimbra, M. O. P. Sampaio, and R. Santos, *Eur. Phys. J.* **C73**, 2428 (2013), 1301.2599.
- [55] R. Costa, M. Mühlleitner, M. O. P. Sampaio, and R. Santos, *JHEP* **06**, 034 (2016), 1512.05355.
- [56] ATLAS, CMS, G. Aad *et al.*, *Phys. Rev. Lett.* **114**, 191803 (2015), 1503.07589.
- [57] P. Bechtle, O. Brein, S. Heinemeyer, G. Weiglein, and K. E. Williams, *Comput. Phys. Commun.* **181**, 138 (2010), 0811.4169.
- [58] P. Bechtle, O. Brein, S. Heinemeyer, G. Weiglein, and K. E. Williams, *Comput. Phys. Commun.* **182**, 2605 (2011), 1102.1898.
- [59] P. Bechtle *et al.*, *Eur. Phys. J.* **C74**, 2693 (2014), 1311.0055.
- [60] ATLAS, M. Aaboud *et al.*, *Eur. Phys. J.* **C78**, 293 (2018), 1712.06386.
- [61] A. Djouadi, J. Kalinowski, and M. Spira, *Comput. Phys. Commun.* **108**, 56 (1998), hep-ph/9704448.
- [62] A. Djouadi, J. Kalinowski, M. Muehleitner, and M. Spira, *Comput. Phys. Commun.* **238**, 214 (2019), 1801.09506.
- [63] G. Belanger, F. Boudjema, A. Pukhov, and A. Semenov, *Comput. Phys. Commun.* **176**, 367 (2007), hep-ph/0607059.
- [64] G. Belanger, F. Boudjema, A. Pukhov, and A. Semenov, *Comput. Phys. Commun.* **177**, 894 (2007).
- [65] G. Belanger, F. Boudjema, A. Pukhov, and A. Semenov, (2010), 1005.4133.
- [66] G. Belanger, F. Boudjema, A. Pukhov, and A. Semenov, *Comput. Phys. Commun.* **185**, 960 (2014), 1305.0237.
- [67] Planck, P. A. R. Ade *et al.*, *Astron. Astrophys.* **594**, A13 (2016), 1502.01589.
- [68] XENON, E. Aprile *et al.*, *Phys. Rev. Lett.* **119**, 181301 (2017), 1705.06655.
- [69] XENON, E. Aprile *et al.*, (2018), 1805.12562.
- [70] CRESST, G. Angloher *et al.*, *Eur. Phys. J.* **C76**, 25 (2016), 1509.01515.
- [71] SuperCDMS, R. Agnese *et al.*, *Phys. Rev. Lett.* **116**, 071301 (2016), 1509.02448.
- [72] G. Bélanger, F. Boudjema, A. Goudelis, A. Pukhov, and B. Zaldivar, *Comput. Phys. Commun.* **231**, 173 (2018), 1801.03509.
- [73] J. Pumplin *et al.*, *JHEP* **07**, 012 (2002), hep-ph/0201195.